

NANO EXPRESS

Open Access



# Lattice Dynamics of the Rhenium and Technetium Dichalcogenides

Daniel Wolverson\* and Lewis S. Hart

## Abstract

The rhenium and technetium dichalcogenides are layered van der Waals semiconductors which show a large number of Raman-active zone-centre phonon modes as a result of their unusually large unit cells and deviation from hexagonal symmetry. They thus offer the possibility of introducing in-plane anisotropy into composite heterostructures based on van der Waals materials, and Raman spectroscopy is generally used to determine their in-plane orientation. We show that first-principles calculations give a good description of the lattice dynamics of this family of materials and thus predict the zone-centre phonon frequencies and Raman activities of  $\text{TcS}_2$ . We consider the distribution of the phonon modes in frequency and their atomic displacements and give a unified understanding of the phonon frequencies and Raman spectra of  $\text{ReS}_2$ ,  $\text{TcS}_2$  and  $\text{ReSe}_2$  in terms of the scaling of Raman frequency with the chalcogen mass.

**Keywords:** Rhenium sulphide, Technetium sulphide, Rhenium selenide, Transition metal dichalcogenide, Raman spectroscopy

## Background

The transition metal dichalcogenides (TMD) have been known for a considerable time; the basic properties of about 40 members of the family were reviewed in 1969 [1]. However, the enormous fundamental scientific interest generated by the isolation of graphene, and the potentially disruptive technologies based on it, has stimulated interest in the wider family of two-dimensional layered van der Waals materials, to which the TMDs belong, with some 2500 publications on the archetypal family member  $\text{MoS}_2$  alone in 2015. This level of activity is likely to be sustained as researchers develop the concept of devices based on multi-layered structures [2] in which dissimilar materials are stacked to achieve new functionalities, for instance, as light emitters [3, 4]. The key to this approach is the wide variety of behaviors that the TMDs exhibit, with metallic, semiconducting and superconducting phases, with properties that can be tuned by doping, and with novel types of coupling between spin and valley physics [5]. Here, we consider some of the less well-studied TMDs, based on Re and Tc, which are also attracting growing interest.

The rhenium and technetium dichalcogenides are layered van der Waals semiconductors with large unit cells

due to their deviation from hexagonal symmetry towards a distorted  $1T'$  structure with space group  $\bar{P}1$  in which the metal atoms group into parallelograms of four atoms [6–8]. They thus offer the unusual possibility of introducing a built-in planar anisotropy into composite heterostructures. Clearly, if their anisotropy is to be useful, one must be able to determine their in-plane orientation, and one promising method for this is Raman spectroscopy [9] since the large unit cell and lack of symmetry-related degeneracies leads to a large number (18) of Raman-active zone-centre phonon modes [9, 10].

It has already been shown that first-principles calculations can give a good description of the lattice dynamics of this family of materials [9, 10]; here, we compare predictions of the phonon frequencies of  $\text{ReS}_2$ ,  $\text{TcS}_2$  and  $\text{ReSe}_2$ . The zone-centre phonon modes show a common distribution in frequency, and we give a simple interpretation of this in terms of the atomic displacements, which leads to a unified understanding of the Raman spectra of  $\text{ReS}_2$ ,  $\text{TcS}_2$  and  $\text{ReSe}_2$ .

Little is known directly about crystalline  $\text{TcS}_2$  though its structure is known [6, 8] and its electronic band structure has been predicted via density functional theory [11–13]. Technetium is not found naturally on Earth but only occurs as a by-product of nuclear fission of uranium-235; all its isotopes are unstable. The most readily available

\*Correspondence: d.wolverson@bath.ac.uk  
Department of Physics, University of Bath, Claverton Down, Bath, UK

isotope,  $^{99m}\text{Tc}$ , is used in nuclear medicine as a radio-pharmaceutical for labeling applications and is highly radioactive with a half-life of  $\sim 6$  h. In that context, it is sometimes produced in the form of a colloid with rhenium sulphide [14]. A longer-lived isotope is  $^{99}\text{Tc}$  (half-life  $2.13 \times 10^5$  years), and the planning of long-term control and storage for this radionuclide in a water-insoluble form is a priority. One proposed strategy involves sequestration of  $^{99}\text{Tc}$  by the formation of its sulphides [15]. For both these applications, a knowledge of the Raman spectrum of  $\text{TcS}_2$  should provide a useful analytic and diagnostic tool. We therefore also present a prediction of the Raman-active modes of  $\text{TcS}_2$  and show how these relate to those of the analogous rhenium compounds.

### Methods

Raman spectra in a backscattering geometry were obtained for the rhenium dichalcogenides using a Renishaw InVia Raman microscope with a  $\times 50$  objective lens giving a laser spot size of around  $1 \mu\text{m}$  with, typically,  $100 \mu\text{W}$  of 532-nm excitation; this microscope also provided the images of the samples in Fig. 1. The preparation (by micro-mechanical cleavage) and characterization of the  $\text{ReSe}_2$  samples is described elsewhere [9], and the  $\text{ReS}_2$  sample was prepared similarly. The  $\text{ReSe}_2$  sample was a few unit cells in thickness whereas the  $\text{ReS}_2$  sample was thicker; the differences between monolayer, few-layer and bulk Raman spectra of these materials are small [9, 10], being much less significant than in the case of  $\text{MoS}_2$ , for example, but have recently been shown to vary systematically with thickness, as do the interlayer modes [16–19].

Calculations of phonon frequencies were carried out using density functional perturbation theory [20] (DFPT) as implemented in the Quantum Espresso code [21]. Initial atomic coordinates were taken from earlier X-ray diffraction studies [7, 8] and were relaxed to reduce the atomic forces below  $10^{-3} \text{ eV/\AA}$ . We have explored the use of norm-conserving pseudopotentials (NCPP) and also the projector augmented wave (PAW) method within both the local density (LDA) and generalized gradient (GGA) approximations; the resulting phonon frequencies given by these methods vary by less than  $\pm 2\%$  and are in good agreement with experiment, as found by other authors [10, 22]. The criteria for the convergence of the total energy with respect to kinetic energy cutoffs (here typically 680 eV) and  $k$ -point grid size (typically  $6 \times 6 \times 6$  for 3D or  $6 \times 6 \times 1$  for 2D) were discussed earlier [9]. Since the bulk unit cell of  $\text{ReS}_2$  may be doubled along the out-of-plane axis [8] (that is, the unit cell may contain two layers), we calculated the phonon modes for an isolated monolayer with a single layer per supercell, so as to obtain the same number of modes and thus facilitate

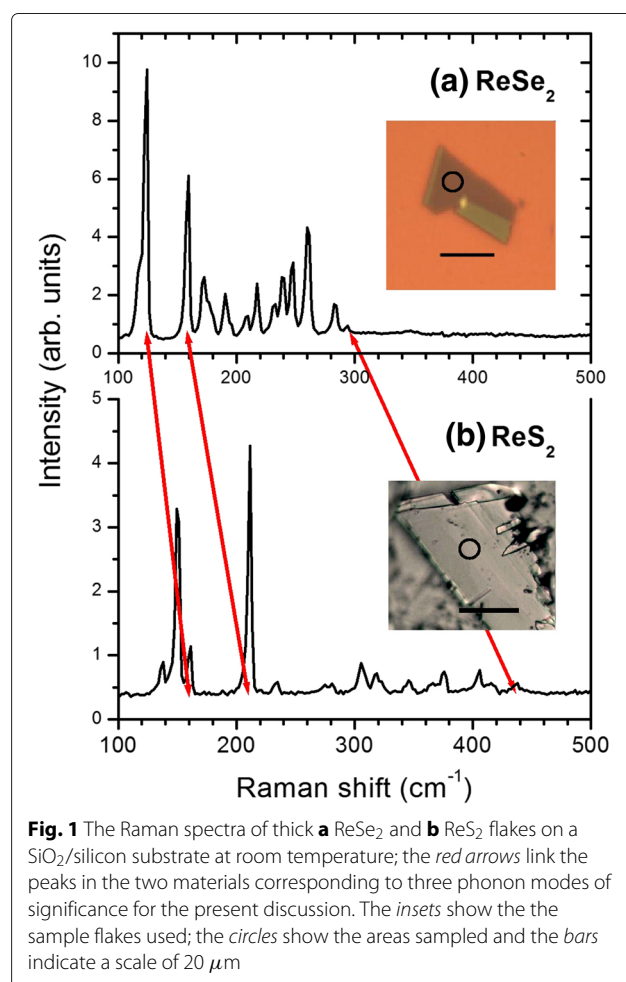


**Fig. 1** The Raman spectra of thick **a**  $\text{ReSe}_2$  and **b**  $\text{ReS}_2$  flakes on a  $\text{SiO}_2/\text{silicon}$  substrate at room temperature; the *red arrows* link the peaks in the two materials corresponding to three phonon modes of significance for the present discussion. The *insets* show the the sample flakes used; the *circles* show the areas sampled and the *bars* indicate a scale of  $20 \mu\text{m}$

comparison. Since the differences between the phonon modes of monolayers and multiple layers are small for a transition metal dichalcogenide [10, 23], this procedure is justified. We note also that this question is not resolved, and one group saw no evidence of doubling of the unit cell for  $\text{ReS}_2$  [24].

### Results and Discussion

Figure 1 shows representative spectra of  $\text{ReSe}_2$  and  $\text{ReS}_2$ ; most of the 18 expected Raman-active  $A_g$  modes can be seen and, as has been described in detail before, the peak intensities are a function of the angle of orientation between the excitation laser polarization and the in-plane crystal axes [9, 18]. For these low-symmetry materials, all components of the Raman tensors for each  $A_g$  mode are non-zero, so that all Raman-active modes have a finite intensity at any angle, but the maximum intensities of different modes occur at different angles. The modes are densely spaced in frequency, but for both materials there is a noticeable “gap” in the spectrum between the 9th and 10th modes as indicated by the red

arrows in Fig. 1 (the higher red arrow links the positions of the highest-frequency Raman-active modes). This makes the two modes in either side of this gap easy to recognize even when weak; they are also found to be amongst the strongest modes in the Raman spectrum [25–28], and so have been a focus of other studies, where they are sometimes labelled as  $E_{2g}$ -like and  $A_{1g}$ -like by analogy with  $\text{MoS}_2$  [10]; the  $E_{2g}$ -like modes are identified because they have significant in-plane displacements, which would twofold degenerate in hexagonal symmetry, and the modes that have displacements with components predominantly normal to the plane would be non-degenerate and are  $A_{1g}$ -like.

We focus on the two modes either side of the gap in the following. In Table 1, we give the frequencies of the Raman-active  $A_g$  modes nearest to the gap limits (these are the 8th or 9th and 10th or 11th modes), and the highest frequency Raman-active mode (35th or 36th), and compare to our experimental values. The indices at which  $A_u$  (IR) and  $A_g$  (Raman) modes occur are not exactly the same for the set of materials or even for the same material with different choices of (for example) pseudopotential, because close-lying  $A_u$  and  $A_g$  modes can sometimes exchange positions in the sequence. Note that calculations of the phonon dispersion of  $\text{ReS}_2$  show that the gap is not a bandgap, in that it does not extend over the whole Brillouin zone [10], but it is an important and reproducible feature at the zone center. A recent calculation of the phonon dispersion of  $\text{TcS}_2$  used a  $2 \times 2 \times 1$  supercell, which yields a somewhat better accuracy in the phonon frequencies than the present approach but folds several modes into the range of the gap and so masks its existence in the zone-centre Raman modes [13].

To summarize the DFPT predictions, we plot in Fig. 2 the calculated frequencies of the 33 zone-centre vibrational modes (18  $A_g$  and 15  $A_u$ ) in order of increasing frequency. The gap occurs in all three materials at the same position, between the 9th and 10th modes, emphasizing the strong similarity between these three compounds. The modes of the sulphides however cover a larger frequency range than those of the selenide, as one would expect based on the lower mass of sulphur (32.065) compared to selenium (78.96), and the frequencies of the Tc and Re sulphides are closely similar well above the gap but different

**Table 1** Calculated zone-centre phonon frequencies of gap-edge and highest Raman-active modes ( $\text{cm}^{-1}$ )

| Mode          | $\text{TcS}_2$<br>calc. | $\text{ReS}_2$<br>calc. | $\text{ReS}_2$<br>expt. | $\text{ReSe}_2$<br>calc. | $\text{ReSe}_2$<br>expt. |
|---------------|-------------------------|-------------------------|-------------------------|--------------------------|--------------------------|
| 8 or 9        | 187.9                   | 162.0                   | 161.3                   | 120.9                    | 123.8                    |
| 10 or 11      | 252.3                   | 218.2                   | 211.4                   | 152.0                    | 158.2                    |
| highest $A_g$ | 444.27                  | 440.7                   | 438.5                   | 309.6                    | 293.9                    |

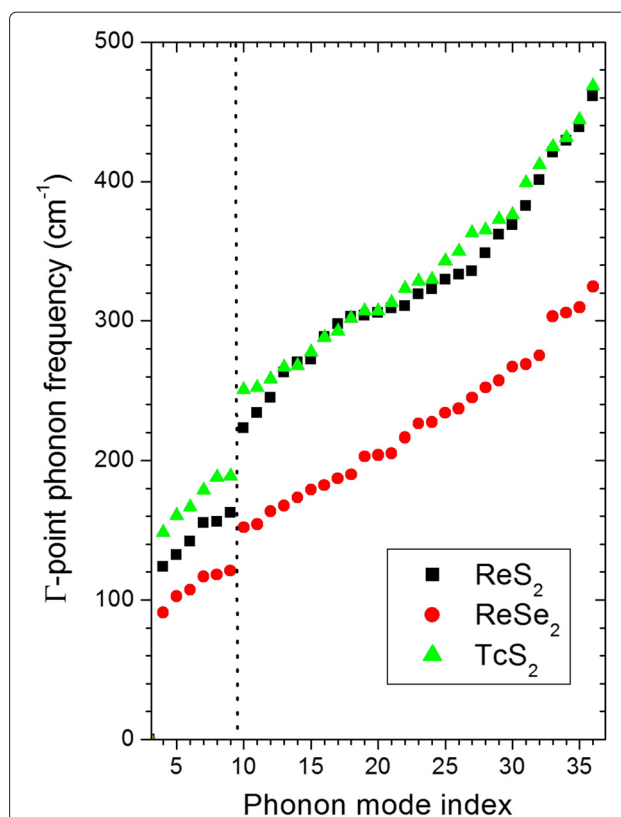


**Fig. 2** The calculated zone-centre phonon modes of  $\text{ReS}_2$  (black squares),  $\text{ReSe}_2$  (red circles) and  $\text{TcS}_2$  (green triangles) plotted in order of increasing frequency. All modes are either IR- or Raman-active. The vertical dotted line indicates the position in frequency of the gap in the phonon spectrum between modes 9 and 10. Note, modes 1–3 are zero-frequency rigid displacements of the unit cell and are not plotted

near and below it. This suggests a simple classification of the modes into those in which the displacements of the metal atoms are significant (mainly below the gap) and those where it is predominantly the chalcogens that are moving (mainly above the gap). By considering the predicted atomic displacements for all modes, we can see that this classification is justified, though there are too many modes to show an exhaustive set of displacements here. As an example, we show in Fig. 3 one view of the predicted displacements for the two gap-edge modes (top and bottom rows, respectively). The displacements of the metal atoms are approximately in-plane and are significant for the lower-frequency mode (8 or 9) but smaller for the higher mode; however, for the higher mode (10 or 11), there are significant out-of-plane displacements of the chalcogen atoms. Similar patterns of phonon displacements were presented earlier for  $\text{ReS}_2$  [10] and, as Fig. 3 shows, the displacement patterns are broadly similar for all three compounds. Concentrating on the displacements of the chalcogen atoms, we can also see the in-plane character of mode 9 ( $E_{2g}$ -like) and the out-of-plane character

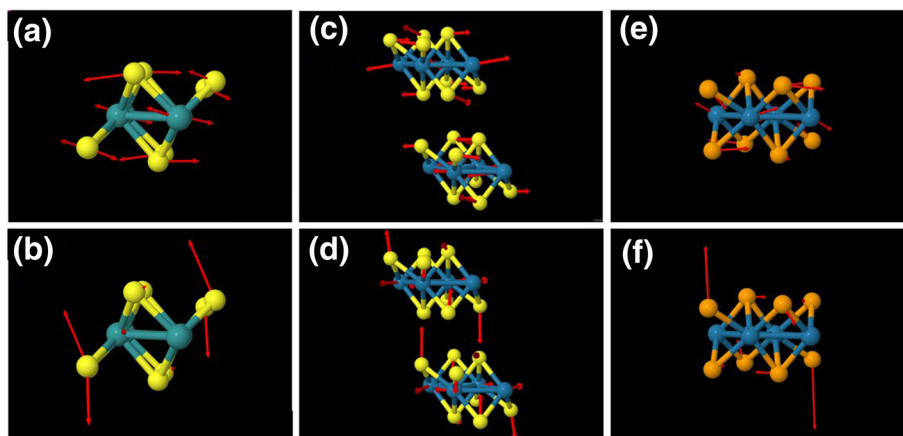


**Fig. 3** The unit cell and phonon displacement vectors (*red*) for  $\text{TcS}_2$  (**a, b**),  $\text{ReS}_2$  (**c, d**) and  $\text{ReSe}_2$  (**e, f**). *Top row*: displacements for the highest frequency mode (mode 9) below the gap and *bottom row*: displacements for the lowest frequency mode above the gap (mode 10). S, yellow; Se, orange; Tc, turquoise; Re, blue

of mode 10 ( $A_{1g}$ -like), in agreement with earlier work [10], and that this is valid also for  $\text{TcS}_2$ .

The similarity of the calculated displacements suggests that the interpretation above is reasonable. To test this further, we make the very simple assumption that, if interatomic “force constants”  $k$  are comparable, the frequencies of corresponding displacement patterns will scale with the square root of the mass  $m$  of the displaced atoms ( $\omega \propto \sqrt{k/m}$ ). For the modes above the gap, this is the chalcogen mass, and therefore, we replot the calculated phonon frequencies in Fig. 4 (top panel) multiplied by  $\sqrt{32.065} = 5.66$  (sulphides) and by  $\sqrt{78.96} = 8.89$  (selenide). The effect of this scaling is dramatic; all three sets of phonon modes now almost coincide above the gap. We can also test the idea that the modes below the gap should scale with the square root of the reduced mass taking into account the metal ions (Fig. 4, bottom panel); the displacement patterns of Fig. 3 suggest that this will not be so successful, because both metal and chalcogen atoms are displaced significantly in the below gap modes. However, by comparison of Fig. 4 with Fig. 2, it is clear that the  $\text{ReS}_2$  and  $\text{TcS}_2$  modes 4–9 now lie closer together.

Finally, in Table 2, the calculated zone-centre phonon frequencies of  $\text{TcS}_2$  are given, since these have not been presented elsewhere. We also give the predicted infrared and Raman activities of these modes, principally to identify the Raman-active modes of the set; it should be noted that the Raman activity given here is the one computed in Quantum Espresso and other packages and represents a specific experimental geometry and an average over all possible sample orientations, as given in Eq. (6) of Porezag et al. [29]. So it does not correspond to the experimental configuration for a cleaved flake supported on a substrate;

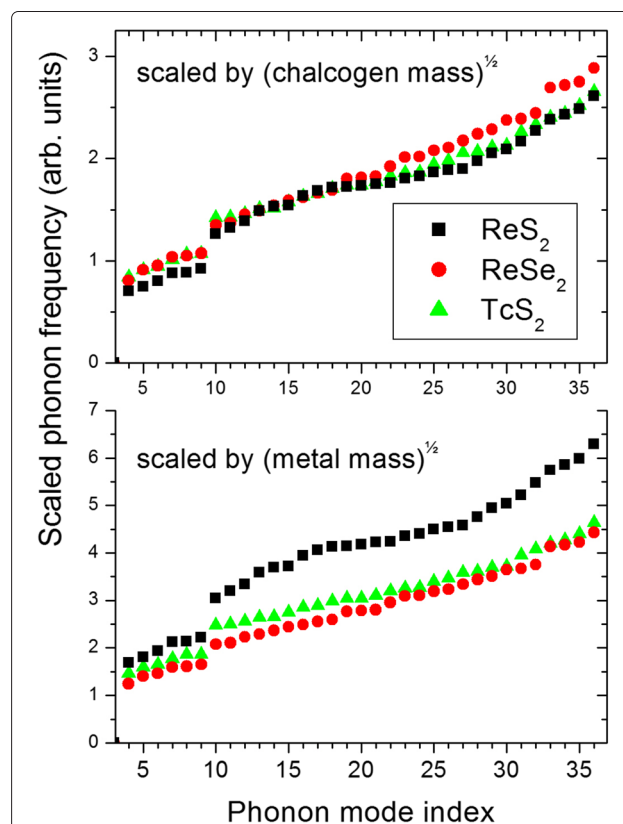


**Fig. 4** The calculated zone-centre phonon modes of  $\text{ReS}_2$  (*black squares*),  $\text{ReSe}_2$  (*red circles*) and  $\text{TcS}_2$  (*green triangles*) plotted in order of increasing frequency and scaled as discussed. *Top*: scaled by the square root of the chalcogen mass; *bottom*: scaled by the square root of the transition metal mass

**Table 2** Calculated zone-centre phonon frequencies of TcS<sub>2</sub>

| Index | Frequency (cm <sup>-1</sup> ) | IR Activity | Raman Activity |
|-------|-------------------------------|-------------|----------------|
| 4     | 148.14                        | 0.0000      | 428            |
| 5     | 160.38                        | 0.0000      | 1016           |
| 6     | 166.40                        | 0.0484      | 0              |
| 7     | 178.54                        | 0.0000      | 3964           |
| 8     | 187.93                        | 0.0000      | 900            |
| 9     | 188.51                        | 0.1416      | 0              |
| 10    | 250.77                        | 0.3533      | 0              |
| 11    | 252.28                        | 0.0000      | 3967           |
| 12    | 258.18                        | 0.3939      | 0              |
| 13    | 266.53                        | 0.0000      | 505            |
| 14    | 267.82                        | 1.2843      | 0              |
| 15    | 277.76                        | 0.0000      | 806            |
| 16    | 287.93                        | 0.3621      | 0              |
| 17    | 292.34                        | 0.0000      | 4655           |
| 18    | 301.69                        | 0.0000      | 2999           |
| 19    | 306.90                        | 0.1785      | 0              |
| 20    | 307.26                        | 0.0000      | 3179           |
| 21    | 312.84                        | 0.0000      | 2761           |
| 22    | 323.05                        | 1.6289      | 0              |
| 23    | 328.50                        | 0.0000      | 1318           |
| 24    | 329.73                        | 4.2948      | 0              |
| 25    | 343.13                        | 2.9997      | 0              |
| 26    | 349.84                        | 0.0000      | 4650           |
| 27    | 362.87                        | 0.1476      | 0              |
| 28    | 365.12                        | 0.0000      | 961            |
| 29    | 372.55                        | 0.2031      | 0              |
| 30    | 375.97                        | 0.0000      | 5592           |
| 31    | 399.18                        | 0.3195      | 0              |
| 32    | 411.93                        | 0.0000      | 6409           |
| 33    | 424.81                        | 0.0000      | 19,660         |
| 35    | 444.27                        | 0.0000      | 9908           |
| 36    | 468.57                        | 3.9835      | 0              |

however, it would be relevant to the measurements on a polycrystalline or colloidal sample, the forms in which TcS<sub>2</sub> is likely to be available.

## Conclusions

We have shown that a simple argument based on scaling by chalcogen mass allows one to understand the zone centre phonon modes of the rhenium and technetium dichalcogenides in a unified way and to understand qualitatively the distribution of the modes in frequency. This emphasizes the strong similarity between the members of this family of materials. The good agreement between

the predicted and experimental frequencies of the Raman bands of the rhenium dichalcogenides gives us confidence in the behavior predicted for the technetium dichalcogenides, and this may be of use in monitoring the chemical composition of technetium-containing suspensions and colloids.

## Competing Interests

The authors declare that they have no competing interests.

## Authors' Contributions

DW conceived the project and carried out the computational work; both authors carried out the experimental work. Both authors read and approved the final manuscript.

## Acknowledgements

This work was supported by the Centre for Graphene Science of the Universities of Bath and Exeter, funded by the EPSRC (UK) under grants EP/G036101 and EP/M0022188; LH is supported by the Bath/Bristol Centre for Doctoral Training in Condensed Matter Physics, grant EP/L015544. Computational work was performed on the University of Bath's High Performance Computing Facility. Data created during this research are freely available from the University of Bath data archive at DOI:10.15125/BATH-00130.

Received: 24 March 2016 Accepted: 2 May 2016

Published online: 13 May 2016

## References

- Wilson JA, Yoffe AD (1969) The transition metal dichalcogenides: discussion and interpretation of the observed optical, electrical and structural properties. *Adv Phys* 18(73):193–335
- Geim AK, Grigorieva IV (2013) van der Waals heterostructures. *Nature* 499(7459):419–425
- Wang X, Xia F (2015) van der Waals heterostructures: stacked 2D materials shed light. *Nat Mater* 14(3):264–265
- Withers F, Del Pozo-Zamudio O, Schwarz S, Dufferwiel S, Walker PM, Godde T, Rooney AP, Gholinia A, Woods CR, Blake P, Haigh SJ, Watanabe K, Taniguchi T, Aleiner IL, Geim AK, Fal'ko VI, Tartakovskii AI, Novoselov KS (2015) WSe<sub>2</sub> light-emitting tunneling transistors with enhanced brightness at room temperature. *Nano Lett* 15(12):8223–8228
- Xiao D, Liu GB, Feng WX, Xu XD, Yao W (2012) Coupled spin and valley physics in monolayers of MoS<sub>2</sub> and other group-VI dichalcogenides. *Phys Rev Lett* 108(19):196802
- Wildervanck JC, Jellinek F (1971) The dichalcogenides of technetium and rhenium. *J Less-Common Metals* 24(1):73–81
- Murray HH, Keltly SP, Chianelli RR, Day CS (1994) Structure of rhenium disulfide. *Inorg Chem* 33(19):4418–4420
- Lamfers HJ, Meetsma A, Wiegers GA, deBoer JL (1996) The crystal structure of some rhenium and technetium dichalcogenides. *J Alloys Compounds* 241(1-2):34–39
- Wolverson D, Crampin S, Kazemi AS, Ilie A, Bending SJ (2014) Raman spectra of monolayer, few-layer, and bulk ReSe<sub>2</sub>: an anisotropic layered semiconductor. *ACS Nano* 8(11):11154–11164
- Tongay S, Sahin H, Ko C, Luce A, Fan W, Liu K, Zhou J, Huang YS, Ho CH, Yan J, Ogletree DF, Aloni S, Ji J, Li S, Li J, Peeters FM, Wu J (2014) Monolayer behaviour in bulk ReS<sub>2</sub> due to electronic and vibrational decoupling. *Nat Commun* 5:3252
- Fang CM, Wiegers GA, Haas C, deGroot RA (1997) Electronic structures of ReS<sub>2</sub>, ReSe<sub>2</sub> and TcS<sub>2</sub> in the real and the hypothetical undistorted structures. *J Phys Condensed Matter* 9(21):4411–4424
- Weck PF, Kim E, Czerwinski KR (2013) Semiconducting layered technetium dichalcogenides: insights from first-principles. *Dalton Trans* 42(43):15288–15295
- Jiao Y, Zhou L, Ma F, Gao G, Kou L, Bell JM, Sanvito S, Du A (2016) Predicting single-layer technetium dichalcogenides (TcX<sub>2</sub>, X= S, Se) with promising applications in photovoltaics and photocatalysis. *ACS Appl Mater Interfaces* 8(8):5385–5392
- Koizumi M, Nomura E, Yamada Y, Takiguchil T, Tanaka K, Yoshimoto M, Makita M, Sakamoto G, Kasumi F, Ogata E (2003) Sentinel node detection

- using  $^{99m}\text{Tc}$ -rhenium sulphide colloid in breast cancer patients: evaluation of 1 day and 2 day protocols, and a dose-finding study. *Nuclear Med Commun* 24(6):663–670
15. Fan D, Anitori RP, Tebo BM, Tratnyek PG, Lezama Pacheco JS, Kukkadapu RK, Engelhard MH, Bowden ME, Kovarik L, Arey BW (2013) Reductive sequestration of pertechnetate by nano zerovalent iron transformed by abiotic sulfide. *Environ Sci Technol* 47(10):5302–5310
  16. Nagler P, Plechinger G, Schüller C, Korn T (2016) Observation of anisotropic interlayer raman modes in few-layer  $\text{ReS}_2$ . *physica status solidi (RRL)-Rapid Research Letters* 10(2):185–189
  17. Lorchat E, Froehlicher G, Berciaud S (2016) Splitting of interlayer shear modes and photon energy dependent anisotropic raman response in  $n$ -layer  $\text{ReSe}_2$  and  $\text{ReS}_2$ . *ACS Nano* 10(2):2752–2760
  18. Chenet DA, Aslan OB, Huang PY, Fan C, van der Zande AM, Heinz TF, Hone JC (2015) In-plane anisotropy in mono- and few-layer  $\text{ReS}_2$  probed by Raman spectroscopy and scanning transmission electron microscopy. *Nano Lett* 15(9):5667–5672
  19. He R, Yan JA, Yin Z, Ye Z, Ye G, Cheng J, Li J, Lui CH (2016) Coupling and stacking order of  $\text{ReS}_2$  atomic layers revealed by ultralow-frequency raman spectroscopy. *Nano Lett* 16:1404–1409
  20. Baroni S, de Gironcoli S, Dal Corso A, Giannozzi P (2001) Phonons and related crystal properties from density-functional perturbation theory. *Rev Mod Phys* 73:515–562
  21. Giannozzi P, Baroni S, Bonini N, Calandra M, Car R, Cavazzoni C, Ceresoli D, Chiarotti GL, Cococcioni M, Dabo I, Corso AD, de Gironcoli S, Fabris S, Fratesi G, Gebauer R, Gerstmann U, Gougoussis C, Kokalj A, Lazzeri M, Martin-Samos L, Marzari N, Mauri F, Mazzarello R, Paolini S, Pasquarello A, Paulatto L, Sbraccia C, Scandolo S, Sclauzero G, Seitsonen AP, Smogunov A, Umari P, Wentzcovitch RM (2009) Quantum espresso: a modular and open-source software project for quantum simulations of materials. *J Phys Condens Matter* 21(39):395502
  22. Feng Y, Zhou W, Wang Y, Zhou J, Liu E, Fu Y, Ni Z, Wu X, Yuan H, Miao F (2015) Raman vibrational spectra of bulk to monolayer  $\text{ReS}_2$  with lower symmetry. *J Phys Rev B* 92:054110
  23. Zhao H, Wu J, Zhong H, Guo Q, Wang X, Xia F, Yang L, Tan PH, Wang H (2015) Interlayer interactions in anisotropic atomically-thin rhenium diselenide. *Nano Research* 8(11):3651–3661
  24. Ho CH, Huang YS, Liao PC, Tiong KK (1999) Crystal structure and band-edge transitions of  $\text{ReS}_2$ - $x\text{Sex}$  layered compounds. *J Phys Chem Solids* 60(11):1797–1804
  25. Yang S, Tongay S, Yue Q, Li Y, Li B, Lu F (2014) High-performance few-layer  $m$ -doped  $\text{ReSe}_2$  nanosheet photodetectors. *Sci Rep* 4:5442
  26. Taube A, Lapinska A, Judek J, Zdrojek M (2015) Temperature dependence of raman shifts in layered  $\text{ReSe}_2$  and  $\text{SnSe}_2$  semiconductor nanosheets. *Appl Phys Lett* 107(1):13105–13105
  27. Yang S, Wang C, Sahin H, Chen H, Li Y, Li SS, Suslu A, Peeters FM, Liu Q, Li J, Tongay S (2015) Tuning the optical, magnetic, and electrical properties of  $\text{ReSe}_2$  by nanoscale strain engineering. *Nano Lett* 15(3):1660–1666
  28. Keyshar K, Gong Y, Ye G, Brunetto G, Zhou W, Cole DP, Hackenberg K, He Y, Machado L, Kabbani M, et al. (2015) Chemical vapor deposition of monolayer rhenium disulfide ( $\text{ReS}_2$ ). *Adv Mater* 31:4640–4648
  29. Porezag D, Pederson MR (1996) Infrared intensities and Raman-scattering activities within density-functional theory. *Phys Rev B* 54:7830–7836

Submit your manuscript to a SpringerOpen<sup>®</sup> journal and benefit from:

- Convenient online submission
- Rigorous peer review
- Immediate publication on acceptance
- Open access: articles freely available online
- High visibility within the field
- Retaining the copyright to your article

---

Submit your next manuscript at ► [springeropen.com](http://springeropen.com)

---